

Multidimensional Josephson vortices in spin-orbit coupled Bose-Einstein condensates: snake instability and decay through vortex dipoles

A. Gallemí,^{1,2} M. Guilleumas,^{1,2} R. Mayol,^{1,2} and A. Muñoz Mateo¹

¹*Departament d'Estructura i Constituents de la Matèria,*

Facultat de Física, Universitat de Barcelona, E-08028 Barcelona, Spain

²*Institut de Nanociència i Nanotecnologia de la Universitat de Barcelona, IN²UB, E-08028 Barcelona, Spain*

(Dated: March 21, 2016)

We analyze the dynamics of Josephson vortex states in two-component Bose-Einstein condensates with Rashba-Dresselhaus spin-orbit coupling by using the Gross-Pitaevskii equation. In 1D, both in homogeneous and harmonically trapped systems, we report on stationary states containing doubly charged, static Josephson vortices. In multidimensional systems, we find stable Josephson vortices in a regime of parameters typical of current experiments with ⁸⁷Rb atoms. In addition, we discuss the instability regime of Josephson vortices in disk-shaped condensates, where the snake instability operates and vortex dipoles emerge. We study the rich dynamics that they exhibit in different regimes of the spin-orbit coupled condensate depending on the orientation of the Josephson vortices.

PACS numbers: 03.75.Lm, 03.75.Mn, 67.85.-d

I. INTRODUCTION

In the last years, new experimental techniques developed in the field of ultracold atoms have allowed the study of challenging physical phenomena by quantum simulation. Among such techniques, the ability to engineer artificial magnetism by means of synthetic gauge fields [1, 2] is one of the most promising topics. In particular, spin-orbit (SO) coupling can be simulated in Bose-Einstein condensates of ultracold gases (BEC) by laser coupling the momentum and the internal degrees of freedom (pseudo-spin) of neutral particles [3–6]. Both experimental and theoretical research have explored diverse systems, including 2D configurations [7], optical lattices [8, 9], or ring geometries [10, 11]; and new phenomena have been analyzed, such as vortex arrays [12], half-quantum vortex states with Rashba coupling [13], roton instability with Rashba-Dresselhaus one [14], or external Josephson oscillations [15, 16].

In the first experimental realization of SO coupling in BECs, an equal amount of Rashba-Dresselhaus coupling has been implemented in a two-component (pseudospin-1/2) condensate [6]. This system is characterized by an inter-component Raman coupling of frequency Ω , and an intra-component momentum shift $\pm\hbar k_L$. For homogeneous condensates of this kind, it has been theoretically demonstrated that such coupling leads to three different phases, namely, stripe, plane-wave, and single-minimum phases, whose appearance depends on the values of the homogeneous density, inter and intraspecies interaction and the linear, internal coupling between components [14, 17–19].

Since the Raman coupling configures an internal, long Josephson junction [20–22], characteristic effects of Josephson dynamics are expected to occur. In comparison with short Josephson junctions connecting BECs [23–26], the physics of the long Josephson links, focusing on the local properties of the system along a uniform junc-

tion, provides a richer variety of dynamical processes. In these systems, in the absence of spin-orbit coupling ($k_L = 0$), and for small tunneling frequencies, there exist metastable domain walls in the relative phase of the coupled components [27]. Furthermore, 1D condensates admit stationary states with non trivial topology in the relative phase [28, 29], in analogy with fluxon states in superconductors [30]. Such states, referred to as Josephson vortices (JVs), are composed of one soliton in each component and have been analyzed in 1D homogeneous condensates, both in linear [28, 29] and ring geometries [31]. In the presence of spin-orbit coupling ($k_L \neq 0$), the study of solitonic stationary states in 1D systems has found stable JVs in homogeneous settings that persist when a harmonic trap is introduced [32]. In this latter arrangement, 1D solitonic structures have also been dynamically generated by varying the coherent coupling [33]. All of these results have pointed to the existence of equivalent topological structures in multidimensional systems that could be realized in ultracold gas experiments.

In this work we demonstrate the existence of stable multidimensional JVs, in the presence of Rashba-Dresselhaus SO coupling, in harmonically trapped BECs with typical parameters of current experiments with ultracold ⁸⁷Rb atoms. We present JV states, characterized by a deep depletion in the total density profile accompanied by a 2π -phase jump in the relative phase between components, belonging either to the plane-wave or to the single-minimum phases of the SO coupled system. In 1D settings, we also report on static doubly charged JVs, for both homogeneous and harmonically trapped condensates. Besides, we analyze the decay dynamics of multidimensional JVs, which are unstable when the chemical potential is high enough to excite vortex lines in the system. Our results show that the decay scenarios in disk-shaped condensates are different from those of dark solitons in scalar elongated condensates where a single solitonic vortex [34, 35] appears at the final stage of the

decay. In our systems such a role is played by vortex dipoles, one in each condensate component, which are linked by domain walls in the relative phase. We show the subsequent dynamics of the vortex dipoles due to the interplay between the SO coupling and the JV orientation.

In section II we introduce our mean-field model for the spinor condensate and provide the numerical parameters we have used for our simulations. Section III is devoted to analyze the features of solitonic states in 1D systems, which we characterize both in homogeneous and harmonically trapped condensates in the presence of SO coupling. Furthermore, we report on doubly charged Josephson vortex states. In section IV, we present stable multidimensional Josephson vortices and analyze the decay in the unstable cases through snake instability. The dynamics of the emergent vortex dipoles is studied in the different phases of the SO coupled condensate. To sum up, we present our conclusions and perspectives for future work in section V.

II. SYSTEM

We consider two-component condensates in the mean field regime, described by the coupled Gross-Pitaevskii equations (GPE) for the condensate wave function $\Psi(\mathbf{r}, t) = [\Psi_\uparrow(\mathbf{r}, t), \Psi_\downarrow(\mathbf{r}, t)]^T$:

$$\begin{aligned} i\hbar \left(\frac{\partial}{\partial t} - \frac{\hbar k_L}{m} \frac{\partial}{\partial x} \right) \Psi_\uparrow &= (\mathcal{H}_\uparrow + g_{\uparrow\downarrow} |\Psi_\downarrow|^2) \Psi_\uparrow + \frac{\hbar\Omega}{2} \Psi_\downarrow \\ i\hbar \left(\frac{\partial}{\partial t} + \frac{\hbar k_L}{m} \frac{\partial}{\partial x} \right) \Psi_\downarrow &= (\mathcal{H}_\downarrow + g_{\uparrow\downarrow} |\Psi_\uparrow|^2) \Psi_\downarrow + \frac{\hbar\Omega}{2} \Psi_\uparrow, \end{aligned} \quad (1)$$

where $\mathbf{k}_L = (k_L, 0, 0)$ and Ω are the laser wave vector and Raman frequency, respectively, characterizing the spin-orbit coupling, and $\mathcal{H}_i = -\hbar^2/2m \vec{\nabla}^2 + V_{\text{trap}} + g_{ii} |\Psi_i|^2$, with $i = \uparrow, \downarrow$, is the Gross-Pitaevskii Hamiltonian for each single component without density coupling. We will assume that the system stays in the miscible regime [36], having equal intra-component interaction strengths $g = g_{\uparrow\uparrow} = g_{\downarrow\downarrow} = 4\pi\hbar^2 a/m$, with scattering length a , and slightly smaller inter-component one $g_{\uparrow\downarrow} = 4\pi\hbar^2 a_{\uparrow\downarrow}/m \lesssim g$, as it occurs in the hyperfine species of ^{87}Rb atoms. The confinement of the system will be provided by a cylindrically symmetric harmonic trap, $V_{\text{trap}} = m(\omega_\rho^2 \rho^2 + \omega_z^2 z^2)/2$, where $\rho^2 = x^2 + y^2$, defining an aspect ratio $\gamma = \omega_z/\omega_\rho$, and characteristic lengths $a_{ho} = a_\rho = \sqrt{\hbar/m\omega_\rho}$ and $a_z = \sqrt{\hbar/m\omega_z}$. The stationary states of Eq. (1) will be written as $\Psi(\mathbf{r}, t) = \exp(-i\mu t/\hbar) [\psi_\uparrow(\mathbf{r}), \psi_\downarrow(\mathbf{r})]^T$, where μ is the chemical potential, and the number of particles N will be fixed by the wave function normalization $\sum_i \int \psi_i^*(\mathbf{r}) \psi_i(\mathbf{r}) d\mathbf{r} = N$.

The dimensionless SO number $m\Omega/\hbar k_L^2$, which measures the ratio between the energy associated to the linear

coupling $\hbar\Omega/2$ and the recoil energy $E_L = \hbar^2 k_L^2/2m$, determines the features of the whole coupling between the components of the condensate. In the absence of interactions, the ground state of a system with spin-orbit coupling is degenerate for the nonzero momenta $\pm\hbar k_L$, given that the referred coupling parameter fulfills $m\Omega/\hbar k_L^2 < 2$; otherwise, there is a single ground state with zero momentum. In repulsively interacting condensates one can observe a similar trend in the dynamical regimes of the system: the lowest energy state has zero momentum, within the single-minimum (SM) phase, for couplings above $m\Omega_c/\hbar k_L^2 = 2(1 - (g - g_{\uparrow\downarrow})n_T/E_L)$ (where n_T is the total density) and non-zero below such value [19]. However the physics of the nonlinear system is richer, and different dynamical phases can be found for $\Omega < \Omega_c$. For moderate values of the interaction, the ground state can occupy one of the two degenerate energy minima, thus acquiring a non-zero momentum and constant density. This dynamical regime is denominated plane-wave (PW) phase, and it is also characterized by the population imbalance of the ground state. More strikingly, when the interaction increases, the system enters the stripe phase, which shows density modulations as a result of the interference created by the occupation of the two momentum states [7, 37].

In what follows, we select a coherent coupling Ω in order for the system to be either in the single-minimum or the plane-wave regime, where the ground state presents a smooth density profile. As we will see, in these regimes, the 3D Gross-Pitaevskii equation admits JV solutions as excited states. They present a localized depletion of the density along with an associated phase jump for each condensate component. Their appearance can be understood by following a dynamical process in which, for a given k_L , the linear coupling Ω is adiabatically increased. Starting in the stripe phase regime, the length between density peaks increases with Ω , up to some critical value Ω_c , where dark-soliton-like structures evolve from the ground state of the system [33]. Above the critical value, the solitonic structure can persist as an excited state in the other dynamical phases of the system, the SM or the PW phases. Previous works have demonstrated the existence and stability of such excited states for the different phases of a 1D system [32], resembling the features of corresponding states in scalar condensates. Our results demonstrate that, even in 1D systems, there exist additional solitonic configurations proper of two-component condensates. Besides, we report on the existence and stability of JVs in multidimensional settings with parameters typical of current experiments. In particular, we will focus on quasi-2D condensates produced by harmonic traps (with aspect ratio $\gamma = 4$) sharing the transverse frequency $\omega_\rho = 2\pi \times 200$ Hz, a laser wavelength $\lambda_L = \sqrt{2}\pi/k_L = 1064$ nm, a coherent coupling Ω ranging from 10 kHz (inside the PW phase) to 30 kHz (inside the SM phase), and scattering lengths $a = 101.41 a_B$ and $a_{\uparrow\downarrow} = 100.94 a_B$, where a_B is the Bohr radius, corresponding to the hyperfine states $|F = 1, m_F = 0\rangle$ and

$|F = 1, m_F = -1\rangle$ of ^{87}Rb .

III. JOSEPHSON VORTICES IN 1D CONDENSATES

The main properties of static JVs can be easily identified in 1D condensates, where analytic solutions to GPE are available in the absence of SO coupling ($k_L = 0$). Contrary to static dark solitons, JVs, being excited states with lower energy, have complex wave functions that denote the presence of interspecies (spin) currents in the condensate.

A. Without SO coupling

It is instructive to start considering a two-component system with $k_L = 0$. Then, the homogeneous ($V_{\text{trap}} = 0$) GPE (1) admits two type of analytic stationary solitonic solutions (that have been addressed in the literature for the particular case $g_{\uparrow\downarrow} = 0$ [28, 38]), namely a dark soliton state

$$\psi_{\uparrow,\downarrow}^{DS}(x) = \pm \sqrt{n_T} \tanh(x/\xi_\mu), \quad (2)$$

having a density-dependent healing length $\xi_\mu = \hbar/\sqrt{m\mu_{\text{eff}}}$, with $\mu_{\text{eff}} = \mu + \hbar\Omega/2$, and valid for all values of the coherent coupling $\Omega \geq 0$, and a Josephson vortex state

$$\Psi_{\uparrow,\downarrow}^{JV}(x) = \sqrt{n_T} \left(\pm \tanh(x/\xi) + i \sqrt{1 - \frac{2\hbar\Omega}{\mu_{\text{eff}}}} \text{sech}(x/\xi) \right), \quad (3)$$

with a limited range of existence $\mu_{\text{eff}} > 2\hbar\Omega$, and a healing length depending on the coherent coupling $\xi = \hbar/\sqrt{2m\hbar\Omega}$. In both states, the \pm signs stand for the components \uparrow and \downarrow respectively, $n_T = n_\uparrow + n_\downarrow = \mu_{\text{eff}}/(g + g_{\uparrow\downarrow})$ is the constant total density, there is no population imbalance $n_\uparrow = n_\downarrow = n_T/2$, and we have defined μ_{eff} as an effective chemical potential [39], which is related to the condensate density. For every single value of μ_{eff} there exists a unique DS state, but several JVs associated to different values of Ω .

DS states in the absence of SO coupling, Eq. (2), show the same symmetry between condensate components as the ground state, since from $\Psi_\uparrow^{GS} = -\Psi_\downarrow^{GS}$ we get the corresponding spin-antisymmetric solitonic state $\Psi_\uparrow^{DS} = -\Psi_\downarrow^{DS}$. In the case of JVs, they fulfill $\Psi_\uparrow^{JV} = -(\Psi_\downarrow^{JV})^*$, which involves time reversal symmetry along with spin antisymmetry. In the range of coexistence of DSs and JVs, the healing length linked to density is narrower than that associated to the coherent coupling, $\xi_\mu < \xi$, and, as a result, DSs possess higher energy ($\propto \hbar^2/m\xi_\mu^2$) than JVs. This fact affects their stability, making the JVs dynamically stable states all along their range of existence in 1D, and turning DSs into dynamically unstable ones whenever $\mu_{\text{eff}} > 2\hbar\Omega$. As we will

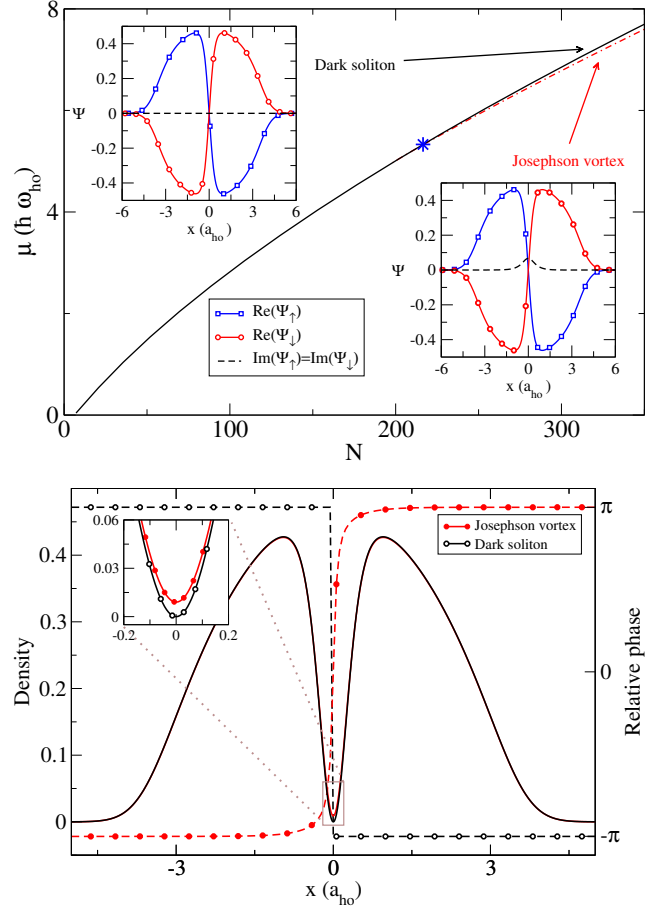


FIG. 1. Family of 1D DS and JV states for two-component condensates, in the absence of SO coupling, confined by a harmonic potential of frequency $\omega_{ho} = 2\pi \times 200$ Hz, and coupled by a Raman frequency $\Omega/\omega_{ho} = 3.5$. Top panel: trajectories in the $\mu - N$ plane (main graph), and two nearby representative examples (insets, DS at the left and JV at the right) corresponding to the (blue) star symbol. Bottom panel: total density (solid line) and relative phase (dashed line) of the DS (open circles) and the JV (filled circles). The inset zooms in the density depleted regions of both cases.

see in the next sections, JVs can decay in multidimensional systems by snake instabilities, in the same manner as DSs do, in spite of the fact that the latter are still more energetic than the former.

The presence of a harmonic trapping potential does not modify qualitatively the type of solitonic solutions in two-component condensates without SO coupling. There also exist stationary states with the same symmetries as those discussed in the homogeneous case (Eqs. (2) and (3)). The main difference arises from the continuation of such solitonic states from the noninteracting regime. Even in this linear case, the system admits both, (real) spin antisymmetric solutions $\Psi_\uparrow = -\Psi_\downarrow$:

$$\psi_{\uparrow,\downarrow}^n(x) = \pm e^{-x^2/2a_{ho}^2} H_n(x/a_{ho}), \quad (4)$$

where H_n is the normalized Hermite polynomial of order

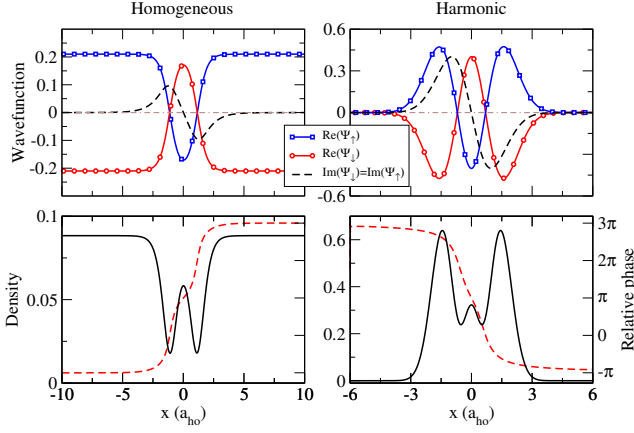


FIG. 2. Doubly charged JVs in homogeneous (left) and trapped (right) settings in the absence of SO coupling. Top panels show the condensate wave functions, and bottom panels depict the total densities (solid lines) and relative phases (dashed lines). For the sake of comparison, the same (harmonic oscillator) units have been used in all the graphs. Homogeneous case: $\mu = 1.77 \hbar \omega_{ho}$, $g_{\uparrow\downarrow} = 0.2 g$, and $\Omega/\omega_{ho} = 0.7$. Trapped case: $\mu = 2.22 \hbar \omega_{ho}$, $g_{\uparrow\downarrow} = 0.9954 g$, and $\Omega/\omega_{ho} = 1.0$.

n , and current states with the stronger symmetry $\Psi_{\uparrow} = -\Psi_{\downarrow}^*$:

$$\psi_{\uparrow,\downarrow}^{n,m}(x) = e^{-x^2/2\xi^2} (\pm\alpha H_n(x/\xi) + i\beta H_m(x/\xi)), \quad (5)$$

where, $n \neq m$, and α and β are real coefficients satisfying $\alpha^2 + \beta^2 = 1$. While states corresponding to Eq. (4) exist, with $\mu_{\text{eff}} = \hbar \omega_{ho}(n + 1/2)$, for every value of Ω , the stronger symmetry of Eq. (5), having $\xi = a_{ho}$, requires that $\Omega = (n - m)\omega_{ho}$, so that $\mu_{\text{eff}} = \hbar \Omega (2n + 1)/2(n - m)$. We have checked that states (4) and (5), which form a big manifold of excited states, persist, and even extend their range of existence, in the nonlinear regime. In particular, the nonlinear families of states starting from $\psi_{\uparrow,\downarrow}^1(x) = \pm e^{-x^2/2a_{ho}^2} H_1(x/a_{ho})$ and $\psi_{\uparrow,\downarrow}^{1,0}(x) = \pm e^{-x^2/2\xi^2} (\pm\alpha H_1(x/\xi) + i\beta H_0(x/\xi))$ are the confined counterpart of the solitonic states Eq. (2) and Eq. (3), respectively. As an example, the top panel of Fig. 1 shows their trajectories in the μ - N plane for $\Omega/\omega_{ho} = 3.5$, and two representative cases (in the insets) for an interaction $g_{1D}N/a_{ho} = 30 \hbar \omega_{ho}$, labeled by a blue star symbol, close to the bifurcation.

As can be seen in the graph of relative phase (bottom panel of Fig. 1), JV states present a 2π -jump characteristic of the sine-Gordon solitons. In fact, it has been shown [27] that the linear equations in the relative phase, obtained by perturbing Eq. (1), admits solutions containing domain walls (or *kinks*) with a length scale that depends on the coherent coupling. The simplest of such solutions, made of a single kink, produces the referred 2π -jump in the relative phase, whereas higher phase jumps can be introduced in the system by generating either several single kinks, or a bound state of a kink and an an-

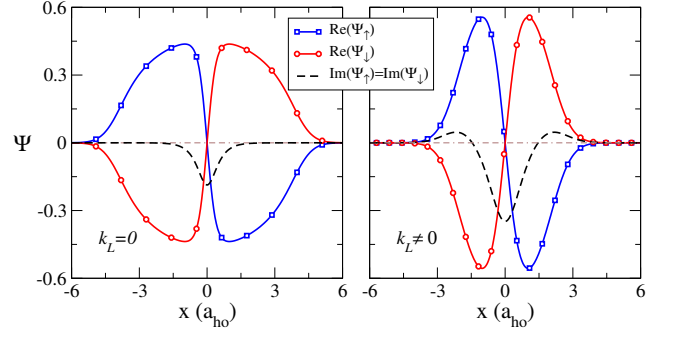


FIG. 3. JVs in the absence ($k_L = 0$) and in the presence ($k_L \neq 0$) of SO coupling for trapped condensates with different parameters. Left: $k_L = 0$, $\Omega/\omega_{ho} = 3.5$, and $\mu = 6.6 \hbar \omega_{ho}$. Right: $a_{ho}k_L = 0.5$, $\Omega/\omega_{ho} = 2$, and $\mu = 1.7 \hbar \omega_{ho}$, within the SM phase. The interaction strengths are the same in both cases, $g_{\uparrow\downarrow} = 0.9954 g$.

tikink (*breather*) [30]. Recently, the dynamical generation of nonlinear excitations resembling the sine-Gordon breathers has been reported in coupled BECs [40]. Here, we show that doubly charged JVs are stationary solutions of the GPE (1), which consist in a bound state of two kinks, making a doubly charged (4π -phase jump) soliton. They can be obtained by introducing additional structure in the core of the JV, where by core we mean the spatial region of the condensate showing a depleted density (see Ref. [41] for JV cores in superconductors). In terms of the singly charged JV (given by Eq. (3)), the core is enclosed in a healing length extension ξ defined by the hyperbolic tangent shape of the wave function (in the homogeneous condensate), and is characterized by a density profile without zeros, described by the hyperbolic secant in the homogeneous case or the Hermite polynomial $H_0(x)$ in the (linear) trapped one. In contrast, a doubly charged JV state must present zeros in the imaginary part of the wave function inside the core, as it is the case of the examples represented in Fig. 2. They correspond to doubly charged JVs for homogeneous and trapped systems, obtained by numerically solving the 1D GPE (1). Both states have no population imbalance. By direct observation of the wave function of the trapped condensate (top right panel), it follows that this state belongs to the family $\psi_{\uparrow,\downarrow}^{2,1}(x) = \pm e^{-x^2/2\xi^2} (\pm\alpha H_2(x/\xi) + i\beta H_1(x/\xi))$.

B. With SO coupling

The laser coupling k_L introduces a significant difference in the nature of the possible solitonic solutions to Eq. (1). Dark solitons of the type described by Eq. (2) are no longer possible, since their symmetry ($\Psi_{\uparrow}^{DS} = -\Psi_{\downarrow}^{DS}$) is not fulfilled by the equation of motion. Contrary to DSs, the symmetry of JVs ($\Psi_{\uparrow}^{JV} = -(\Psi_{\downarrow}^{JV})^*$) is preserved by the SO coupling. The wave functions of JVs, both in the homogeneous and trapped systems, are

very similar to those shown in Fig. 1. The main difference is the appearance of zeros (out of the soliton core) in their imaginary parts, as a result of the relative momentum introduced by $\pm\hbar k_L$. This feature can be seen in Fig. 3, where we have plotted JVs in the absence of SO coupling, on the left, and in the presence of SO coupling, for $a_{ho}k_L = 0.5$, on the right, for two different number of particles and coherent coupling. As it is reported below, multidimensional solitons present the same features (see Fig. 4) discussed below.

IV. JOSEPHSON VORTICES IN MULTIDIMENSIONAL, PANCAKE-SHAPED CONDENSATES

Multidimensional BECs, composed of two coherently coupled (spin) components, can exhibit topological states in correspondence with the 1D ones presented before. In general, their existence depends on the interaction and on the inter-component coupling. As it is detailed below, our numerical results show that in harmonically trapped systems static DSs and JVs can be found in the absence of SO coupling ($k_L = 0$), but only static JVs survives to non-zero values of k_L .

In order to find solitonic states, we evolve the full-3D Gross-Pitaevskii Eq. (1) in imaginary time, from the initial ansatz:

$$\psi_{\uparrow}(\mathbf{r}) = -\psi_{\downarrow}(\mathbf{r}) = \chi_{\perp}(y, z) \tanh(x/\xi(y, z)), \quad (6)$$

where $\chi_{\perp}(x = 0, y, z)$ is a transverse ground state, and $\xi(y, z) = \hbar/\sqrt{mg|\chi_{\perp}|^2}$ a local healing length. This ansatz, which corresponds to a dark soliton state in the x -direction (situated at $x = 0$), follows from the approach proposed in Ref. [35] for scalar condensates, and, apart from being a real function, captures the main features of the solitonic solution (phase jump and density depletion) we are searching for. In particular, for the high-interaction regime it is explicitly defined through the Thomas-Fermi wave function $\chi_{TF} = \sqrt{(\mu_{\text{eff}} - V(x = 0, y, z))/(g + g_{\uparrow\downarrow})}$. In the case of solitons in the y -direction, x and y swap places in Eq. (6). Figure 4 shows a 3D JV in a spin-orbit-coupled system, obtained by following the procedure previously described. The condensate, which contains $N = 500$ ^{87}Rb atoms and is trapped by an external harmonic potential of frequency $\omega_{\rho} = 2\pi \times 200$ Hz and aspect ratio $\gamma = 4$, belongs to the SM phase, having the SO number $m\Omega/\hbar k_L^2 = 2.36$ (with $\Omega = 30$ kHz). This is a stationary solution of the GPE (1) with a non-trivial phase, given by a complex wave function (lower panel of Figure 4) which involves the existence of inter-spin currents in the system. Comparing this state with the 1D JV without SO coupling, represented in Fig. 1, the only difference comes from the zeros (out of the soliton core) in the imaginary part of the wave function.

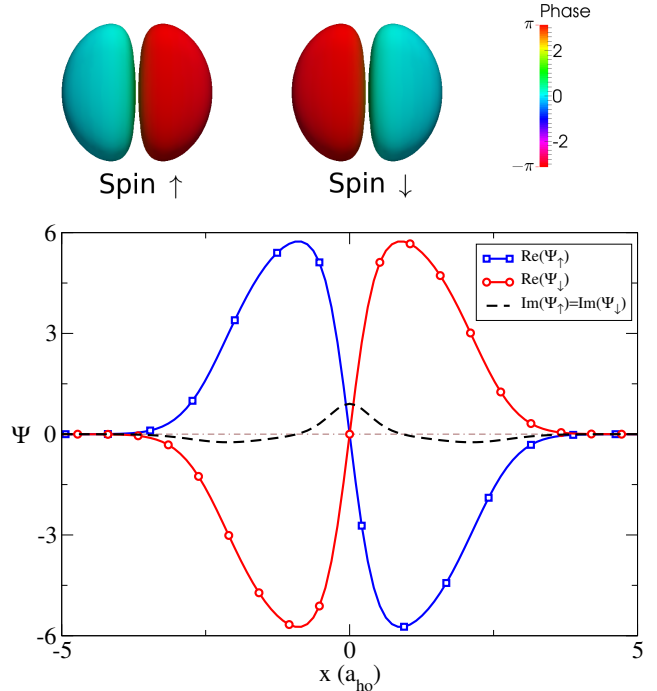


FIG. 4. 3D Josephson vortex in a two-component condensate made of $N = 500$ ^{87}Rb atoms, trapped by a harmonic potential of frequency $\omega_{\rho} = 2\pi \times 200$ Hz and aspect ratio $\gamma = 4$, with a spin-orbit coupling characterized by $\lambda_L = 1064$ nm and $\Omega = 30$ kHz. Top panel: density isocontours of the two components, at 5% of maximum density, coloured by phase. Bottom panel: real (solid) and imaginary (dashed) part of the wave functions (blue squares for spin- \uparrow and red circles for spin- \downarrow) along the x -axis (for $y = z = 0$). The imaginary part of the wave functions for both components are overlapped.

A. Stable Josephson vortices

In the same way as it occurs with DSs in scalar BECs, it is possible to find dynamically stable JV states below an interaction threshold, or equivalently, below a critical value of the effective chemical potential μ_{eff} . Above this, JVs are unstable topological states, whose decay leads to the appearance of vortex lines in the system.

In order to demonstrate the stability of multidimensional JVs, we have analyzed SO coupled condensates in quasi-2D systems. To this aim, we have assumed that the axial degrees of freedom of the 3D system are frozen, in such a way that the corresponding wave function is composed by an axial (z) separable part given by the ground state of the axial harmonic oscillator, that is, $\Psi(x, y, z) = \psi(x, y)\psi_z(z)$, where $\psi_z(z) = \exp(-z^2/2a_z^2)/\sqrt{a_z\sqrt{\pi}}$. After substituting this expression in Eq. (1), multiplying by $\psi_z^*(z)$ and integrating over z , we get an equivalent two-dimensional GPE, where all the interaction strengths (g and $g_{\uparrow\downarrow}$) are renormalized by the factor

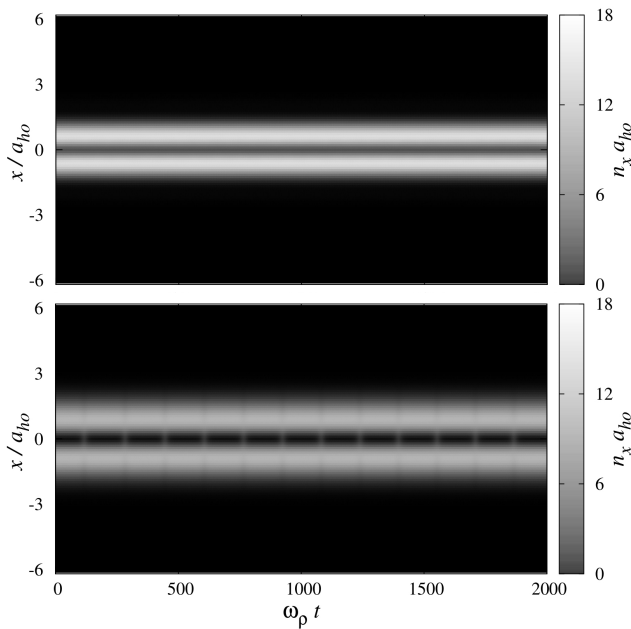


FIG. 5. The top (bottom) panel shows the real time evolution of a JV across the x -direction in a 2D system with SO coupling, for $\Omega = 10$ kHz (30 kHz) inside the the PW (SM) phase. Common parameters: $N_{2D} = 50$, $\omega_\rho = 2\pi \times 200$ Hz, $\gamma = 4$, and $\lambda_L = 1064$ nm.

$$a_z g_{2D}/g = 1/\sqrt{2\pi}.$$

Our results show that the critical value of μ_{eff} for stability depends strongly on the presence of SO coupling, and specifically on the dimensionless number $m\Omega/\hbar k_L^2$. Without SO coupling, and for $\Omega = 30$ kHz, JVs are stable in 2D condensates containing up to $N_{2D} = 250$ particles. Under SO coupling, however, stability is dramatically reduced. Moreover, the richer phase diagram produces differences on the stability for the same μ_{eff} , and provides different dynamical scenarios in the soliton decay.

In Fig. 5 we show the real time evolution of JVs, across the x -direction, in the presence of SO coupling (with the wave vector \mathbf{k}_L also lying on x). For the initial state, at time $t = 0$, we have added a Gaussian noise $\delta(\mathbf{r})$ to the stationary wave function $\psi(\mathbf{r}) \rightarrow \psi(\mathbf{r})[1 + 0.01\delta(\mathbf{r})]$, that we will refer to as 1%-strength noise. The dimensionless density of the spin- \uparrow component, integrated over the coordinate y perpendicular to the soliton, $n_x(x) = \int |\psi_\uparrow(x, y)|^2 dy$, is represented against time, given in harmonic oscillator units. The top panel of Fig. 5 corresponds to a stable JV in a 2D condensate containing $N_{2D} = 50$ atoms, confined by a harmonic trap of frequency $\omega_\rho = 2\pi \times 200$ Hz and aspect ratio $\gamma = 4$. The SO number is $m\Omega/\hbar k_L^2 = 0.79$ (for $\Omega = 10$ kHz), situating the system inside the PW phase. The horizontal dark line halving the atomic cloud marks the position of the JV, which remains unaltered during the whole evolution. The case represented in the bottom panel of Fig. 5 is more peculiar. It has the same parameters as the condensate in the top panel except for a higher coherent

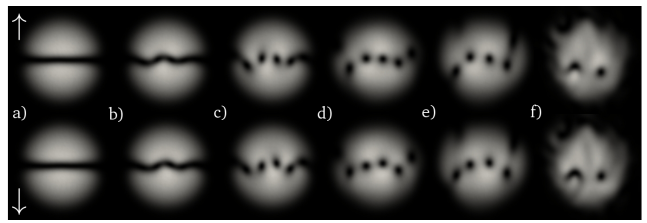


FIG. 6. Decay of a Josephson vortex, in the y -direction of a two-dimensional system with SO coupling, by snake instability of the soliton plane. Condensate parameters: $N_{2D} = 2000$, $\omega_\rho = 2\pi \times 200$ Hz, $\gamma = 4$, $\lambda_L = 1064$ nm, and $\Omega = 30$ kHz. The spin- \uparrow (top) and spin- \downarrow (bottom) density snapshots, from (a) to (f), correspond to times $\omega_\rho t = 3.5, 4.3, 5, 6, 8$, and 20 , respectively. This sequence belongs to the real time evolution shown in Fig. 10.

coupling $\Omega = 30$ kHz, which puts the system within the SM phase with a SO number $m\Omega/\hbar k_L^2 = 2.36$. Small periodic deviations from the initial (perturbed) state can be observed in the graph. Nevertheless, the stationary configuration is rapidly recovered, and the JV persists as a robust state.

B. Decay dynamics

Josephson vortices in multidimensional systems are unstable against transverse modes with long wavelengths. In this sense, the decay of JVs follows qualitatively that of DSs in scalar condensates, by snaking the soliton plane and producing vortex lines inside the system [42]. In elongated condensates, the decay of a DS generates a solitonic vortex [34, 35], which survives as a dynamically stable state. However, in scalar disk-shaped condensates a single vortex can not be generated after the soliton decay, because of angular momentum conservation; instead, a vortex dipole, constituted of a vortex and an antivortex, is left over [43, 44]. As we will demonstrate in what follows, this is also the case for disk-shaped SO coupled condensates. A vortex dipole per component is the remainder of the JV at the last stage of its decay.

Figure 6 shows the whole time sequence of decay, from (a) to (f), for a JV across the y -direction in a ^{87}Rb , 2D condensate containing 2000 atoms. As can be seen, the two components follow a synchronized decay. After the snaking of the soliton plane, several pairs of vortex dipoles appear, almost overlapped, for each spin component. The vortices situated at the same position are connected by domain walls in the relative phase [27]. Finally, only one vortex dipole per component survives, and their subsequent evolution depends both on the particular dynamical regime of the system (i.e. either the SM or PW phase), and on the orientation of the JV plane with respect to the direction of the laser wave vector \mathbf{k}_L .

For the sake of comparison, we consider first the decay dynamics in the absence of SO coupling. In Fig. 7 we show the real time evolution of a stationary JV after

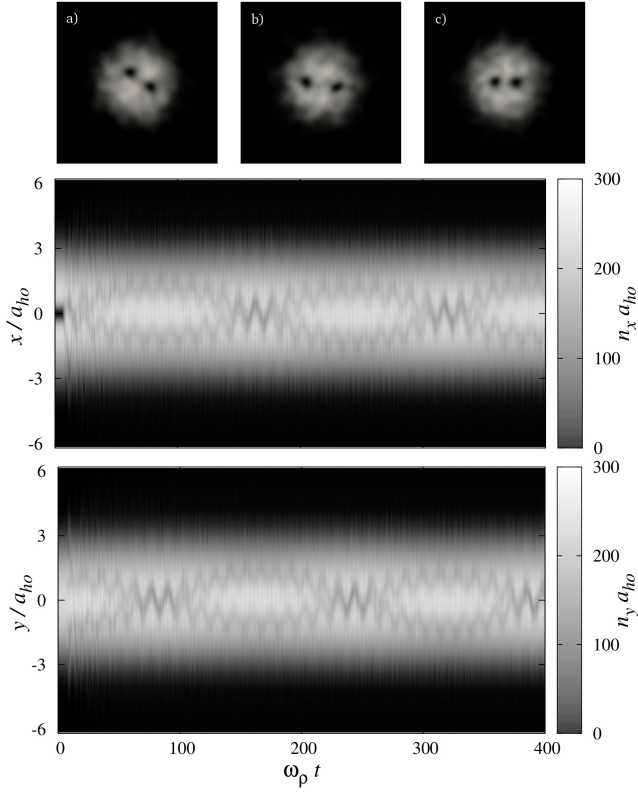


FIG. 7. Real time evolution of a Josephson vortex in the x -direction, in a 2D condensate without SO coupling, and parameters: $N_{2D} = 2000$, $\omega_\rho = 2\pi \times 200$ Hz, $\gamma = 4$, $\lambda_L = 1064$ nm, and $\Omega = 10$ kHz. Upper panel: spin- \uparrow -density snapshots, from (a) to (c), at times $\omega_\rho t = 51, 73$, and 78 , respectively. Middle and lower panels: non-dimensional spin- \uparrow density integrated over the y (middle) and x (bottom) directions.

adding a 1%-strength noise. The two lower panels represent the dimensionless density $a_{ho}n_x(x)$ and $a_{ho}n_y(y)$ for one condensate component (spin- \uparrow). After few $\omega_\rho t$ cycles, the JV (thick black line) decays into a vortex dipole (upper snapshots of Fig. 7) that describes a zigzag path (one per vortex) in the x and y coordinates. The dynamics of the vortex dipole consists in a superposition of a rotation around the center of the trap (low frequency oscillation in the graph), due to the rotational symmetry of the condensate, and a vibration of the relative position of the vortices (high frequency oscillation).

When SO coupling is switched on, the rotational symmetry is broken, and the vortex dipole that appears after the decay of the JV can not rotate freely. The term $-\hat{\mathbf{p}}\Psi \cdot \hbar\mathbf{k}_L$ enters the GPE (1) as the potential of a magnetic dipole $-\boldsymbol{\mu}_S \cdot \mathbf{B}$, where $\boldsymbol{\mu}_S$ is the magnetic moment of a spin-1/2 particle and \mathbf{B} is the static magnetic field. In this way, the velocity of the vortex dipole $-\hat{\mathbf{p}}\psi_\uparrow$, which is perpendicular to the dipole direction, interacts with the SO momentum \mathbf{k}_L , generating an aligning torque given by $\hat{\mathbf{p}}\psi_\uparrow \times \hbar\mathbf{k}_L$. Therefore, the orientation of the JV is crucial for the later dynamics of the emergent vortex dipoles,

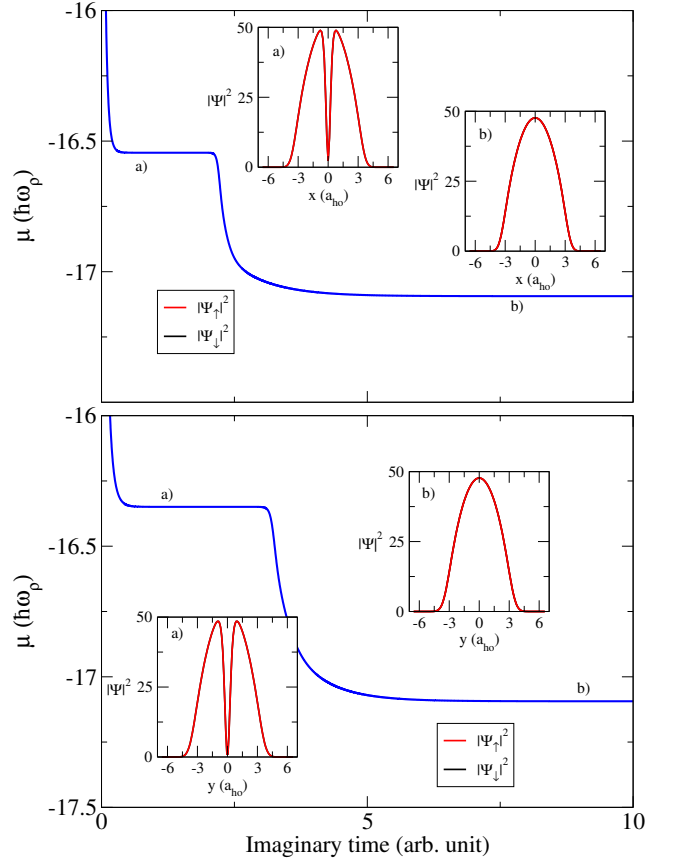


FIG. 8. Imaginary time evolution of JVs, in the x (top) and y (bottom) directions, within the SM phase, with parameters: $N_{2D} = 2000$, $\omega_\rho = 2\pi \times 200$ Hz, $\gamma = 4$, $\lambda_L = 1064$ nm, $\Omega = 30$ kHz. The insets, showing the spin densities along selected axis, correspond to different stationary states, from the initial JV up to the final ground state.

since their alignment follow the JV one. Given that this orientation and the velocity field of the dipoles are the same for both components, the opposite laser momentum $\pm \hbar\mathbf{k}_L$, yields to energies and acting torques with different signs. For this reason, in what follows, we address the decay of JVs in different dynamical regimes, and with different orientations of the soliton plane, along the laser wave vector (x) and perpendicular to it (y).

1. Josephson vortices in the SM phase

In the SM phase, the ground state of the system does not present population imbalance and the density profiles of both condensate components coincide. This is also the case for the excited states containing JVs. As can be seen in Fig. 8, the imaginary-time evolution of our initial ansatz Eq. (6) reaches the energy plateaus of JVs, represented in the insets Fig. 8(a), for the two orientations considered, x in the upper panel of the figure and y in the lower one, before falling to the ground state of the system, depicted in the insets Fig. 8(b). During

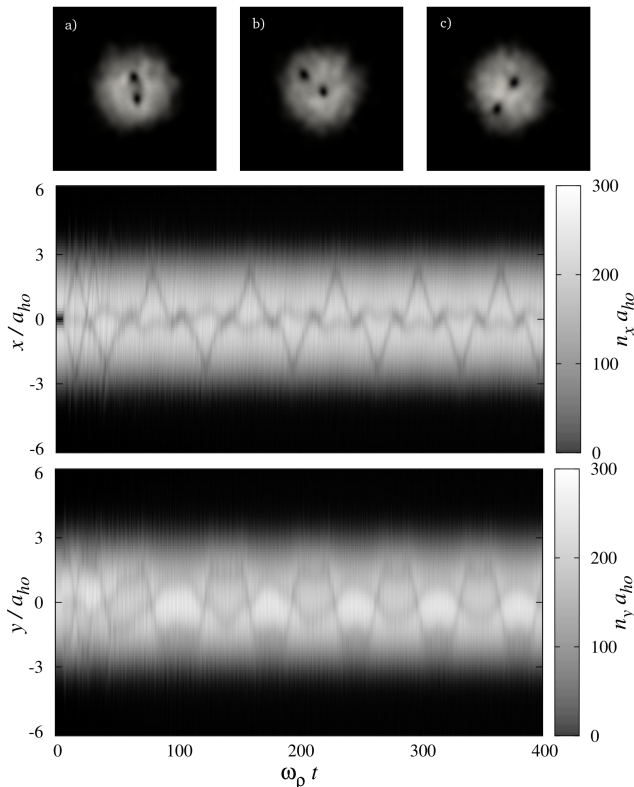


FIG. 9. Real time evolution of the Josephson vortex, in the x -direction, shown in the top panel of Fig. 8. Upper panel: spin- \uparrow -density snapshots, from (a) to (c), at times $\omega_\rho t = 99, 112$, and 124 , respectively. Lower panels: evolution of the non-dimensional spin- \uparrow density integrated over the y (top) and x (bottom) directions.

the whole evolution, obtained for the coherent coupling $\Omega = 30$ kHz and SO number $m\Omega/\hbar k_L^2 = 2.36$, the population imbalance remains at zero.

JV states have a nonzero mean momentum. Therefore, their mean energy depends on their orientation because of the term associated to the SO coupling. As a result, for the same parameters, a JV across the y -direction has higher energy than a JV across x (as can be seen in the main graphs of Fig. 8). In the latter case, the momentum originated by the JV is aligned with the laser wave vector, and then the energy of the system is reduced. On the other hand, for the JV across the y -direction the SO coupling has no influence on the mean energy.

In order to analyze the dynamics of the JVs found in Fig. 8, we have performed their real time evolution by numerically solving the GPE (1), after adding a 1%-strength noise to the respective stationary states. The results are plotted in Fig. 9 for the JV oriented across x , and Fig. 10 for the JV oriented across y . In the former case the velocities of the emerging vortex dipoles are aligned with the laser wave vector. One of the dipoles lays on the energy minimum of the SO potential, whereas the other one occupies the energy maximum. This configuration is unstable and degenerate against exchange of the

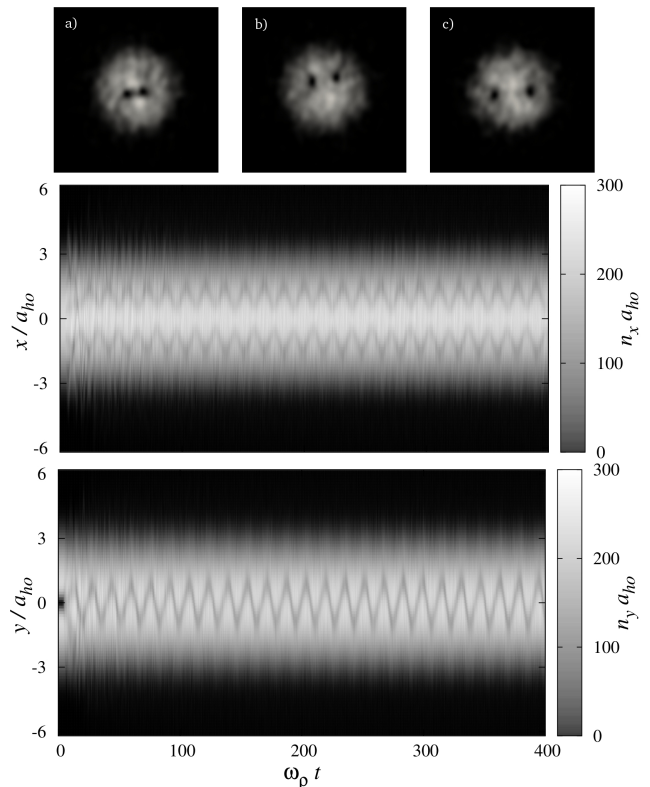


FIG. 10. Same as Fig. 9, for the JV, in the y -direction, shown in the bottom panel of Fig. 8. The snapshots, from (a) to (c), correspond to times $\omega_\rho t = 102, 108$, and 112 , respectively.

positions of the vortex and the anti-vortex. As a consequence, the system oscillates between one configuration and the other. The whole picture can be seen in the evolution of Fig. 9, where the peaked paths correspond to the motion of a vortex around the anti-vortex in order to exchange their positions. When the JV is oriented across y (Fig. 10) the evolution resembles the case without SO coupling, except by the lacking of rotational motion of the dipoles around the center of the trap, because of the absence of rotational symmetry. The vortex dipoles are vibrating along with a small precession, keeping the orientation of the dipoles.

2. Josephson vortices in the PW phase

As commented previously, the PW phase is characterized by a ground state presenting population imbalance. However, the JV states do not share this feature. Then, by evolving a JV in imaginary time it is possible to find new, intermediate excited states before reaching the ground state. Figure 11 represents this evolution for JVs (at insets (a)) across x (top panel) and y (bottom panel), having the coherent coupling $\Omega = 10$ kHz and SO number $m\Omega/\hbar k_L^2 = 0.79$. The evolution finds several plateaus that correspond to solutions of the time-independent ver-

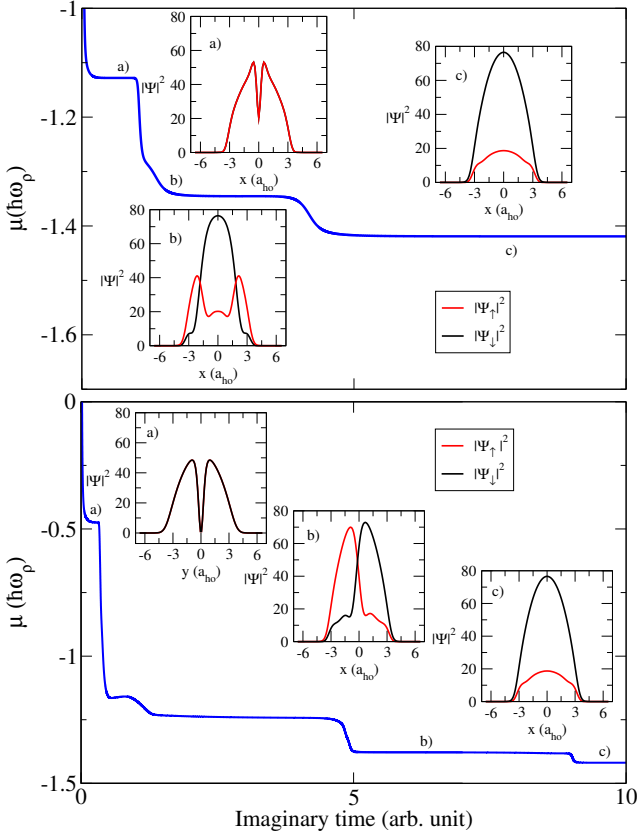


FIG. 11. Same as Fig. 8 for JVs in the PW phase ($\Omega = 10$ kHz).

sion of Eq. (1), and include population imbalance (at insets (b)). At the last stage of the evolution, the ground state is obtained (at insets (c)).

In the PW phase, the JV decay is different to the picture outlined before in Fig. 6. The characteristic population imbalance of the ground state plays a crucial role in the decay dynamics. For the JV across y , a big population imbalance appears, the density of one of the components is highly depleted, and no vortices are finally left over. In contrast, the decay of the JV across x is driven by phase separation. This phenomenon occurs at the first stage through the formation of new solitonic structures during the separation that finally decay into vortices. The resulting configuration presents again vortex dipoles that live near the surface of each condensate component. The vortex dipoles move according to the oscillation of the boundary between components, but their orientation does not change in time because of the alignment of the dipole velocity and the laser wave vector. A whole evolution of this type is represented in Fig. 12, where the integrated density profile of both spin components are shown for the JV across the x -direction of Fig. 11 (inset (a) of the top panel).

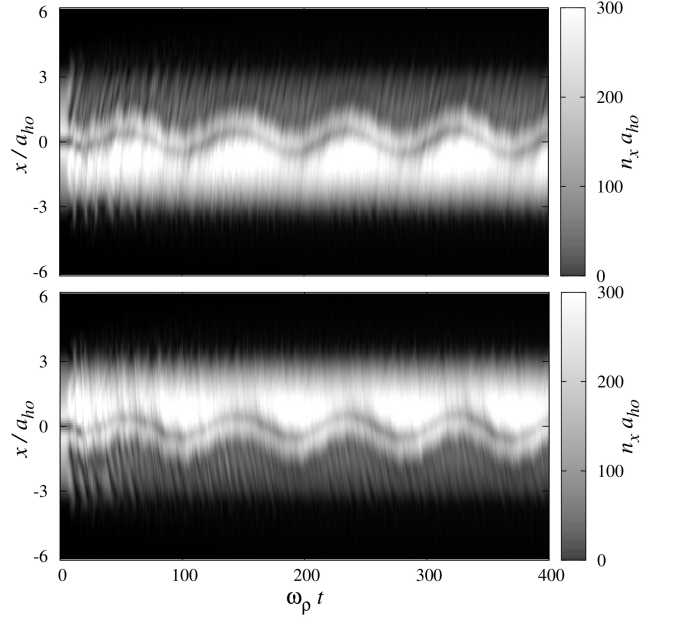


FIG. 12. Real time evolution of the Josephson vortex, in the x -direction, shown in the top panel of Fig. 11. Top (bottom) panel shows the dimensionless, spin- \uparrow (spin- \downarrow) density after integration over the coordinate y .

V. CONCLUSIONS

In this work, we have studied the dynamics of JV states in two-component BECs with Rashba-Dresselhaus SO coupling, by using a mean-field model based in the Gross-Pitaevskii equation. We have considered the appearance of such topological states in a variety of dimensional settings, ranging from 1D systems with different interaction strengths, to 3D condensates in harmonic traps. Regarding the SO coupling, we have focused on systems belonging either to the PW phase, whose ground state presents population imbalance, or to the SM phase, with zero population imbalance.

In 1D systems, both in homogeneous and in harmonically trapped settings, we have reported on stationary states containing doubly charged, static JVs, consisting in a bound state of two JVs. Furthermore, in the trapped case, we have characterized families of nonlinear solitonic states connecting with analytical solutions of the non-interacting system.

In multidimensional systems, by numerically solving the full GPE for disk-shaped settings, we have found stable JVs in a regime of parameters typical of current experiments with ^{87}Rb atoms. In addition, we have also studied the snake instability operating on 2D JVs, which yields to the appearance of vortex dipoles. Due to the interaction between the SO wave vector, which breaks the rotational symmetry of the system, and the dipole velocities, the subsequent evolution sharply changes with respect to that of two-component condensates without SO coupling. Our results show how the JV decay leads

to different scenarios depending, on the one hand, on the orientation of the initial JV, and, on the other hand, on the dynamical phase (PW or SM) of the system. As a future direction, and beyond the scope of the present work, a more detailed analysis concerning the appearance of instability modes, and the generation of alternative solitonic states, would be worth of being done.

Finally, we want to emphasize the feasibility of the multidimensional JV states presented in this work for their experimental realization, either in the stable or in the unstable regime. The latter, in particular, opens up an interesting way to study the snake instability in two-component condensates, in the same manner as it is currently being the case of DS decay in scalar condensates

[45, 46]. Besides, the decay of JVs in SO coupled condensates provides an excellent playground to investigate the rich dynamics of vortex dipoles as has been previously done in scalar BECs [47, 48].

ACKNOWLEDGMENTS

We acknowledge financial support from the Spanish MINECO (FIS2011-28617-C02-01 and FIS2014-52285-C2-1-P) and the European Regional development Fund, Generalitat de Catalunya Grant No. 2014 SGR 401. A.G. is supported by Spanish MECD fellowship FPU13/02106.

-
- [1] J. Dalibard, F. Gerbier, G. Juzeliunas, and P. Ohberg, *Rev. Mod. Phys.* **83**, 1523 (2011).
 - [2] N. Goldman, G. Juzeliunas, P. Ohberg, and I. B. Spielman, *Rep. Prog. Phys.* **77**, 126401 (2014).
 - [3] T. D. Stanescu, B. Anderson, and V. Galitski, *Phys. Rev. A* **78**, 023616 (2008).
 - [4] Y.-J. Lin, R. L. Compton, K. Jiménez-García, J. V. Porto, and I. B. Spielman, *Nature* **462**, 628 (2009).
 - [5] Y.-J. Lin, K. Jiménez-García, and I. B. Spielman, *Nature* **471**, 83 (2011).
 - [6] V. Galitski and I. B. Spielman, *Nature* **494**, 49 (2013).
 - [7] S. Sinha, R. Nath, and L. Santos, *Phys. Rev. Lett.* **107**, 270401 (2011).
 - [8] C. Hamner, Y. Zhang, M. Kamehchi, M. J. Davis, and P. Engels, *Phys. Rev. Lett.* **114**, 070401 (2015).
 - [9] Y. Zhang and C. Zhang, *Phys. Rev. A* **87**, 023611 (2013).
 - [10] X. Chen, M. Rabinovic, B. M. Anderson, and L. Santos, *Phys. Rev. A* **90**, 043632 (2014).
 - [11] F. Mivehvar and D. L. Feder, *Phys. Rev. A* **92**, 023611 (2015).
 - [12] J. Radic, T. A. Sedrakyan, I. B. Spielman, and V. Galitski, *Phys. Rev. A* **84**, 063624 (2011).
 - [13] B. Ramachandran, B. Opanchuk, X.-J. Liu, H. Pu, P. D. Drummond, and H. Hu, *Phys. Rev. A* **85**, 023606 (2012).
 - [14] G. I. Martone, Y. Li, L. P. Pitaevskii, and S. Stringari, *Phys. Rev. A* **86**, 063621 (2012).
 - [15] D.-W. Zhang, L.-B. Fu, Z. D. Wang, and S.-L. Zhu, *Phys. Rev. A* **85**, 043609 (2012).
 - [16] M. A. García-March, G. Mazzarella, L. Dell’Anna, B. Juliá-Díaz, L. Salasnich, and A. Polls, *Phys. Rev. A* **89**, 063607 (2014).
 - [17] Y. Li, L. P. Pitaevskii, and S. Stringari, *Phys. Rev. Lett.* **108**, 225301 (2012).
 - [18] Y. Li, G. I. Martone, and S. Stringari, *Europhys. Lett.* **99**, 56008 (2012).
 - [19] Y. Li, G. I. Martone, and S. Stringari, “Annual review of cold atoms and molecules,” (2015) Chap. SPIN-ORBIT-COUPLED BOSE-EINSTEIN CONDENSATES, p. 201.
 - [20] J. E. Williams and M. J. Holland, *Nature* **401**, 568 (1999).
 - [21] J. E. Williams, R. Walser, J. Cooper, E. A. Cornell, and M. J. Holland, *Phys. Rev. A* **59**, R31(R) (1999).
 - [22] C. Gross, T. Zibold, E. Nicklas, J. Estève, and M. K. Oberthaler, *Nature* **464**, 1165 (2010).
 - [23] A. Smerzi, S. Fantoni, S. Giovanazzi, and S. R. Shenoy, *Phys. Rev. Lett.* **79**, 4950 (1997).
 - [24] S. Raghavan, A. Smerzi, S. Fantoni, and S. R. Shenoy, *Phys. Rev. A* **59**, 620 (1999).
 - [25] M. Albiez, R. Gati, J. Fölling, S. Hunsmann, M. Cristiani, and M. K. Oberthaler, *Phys. Rev. Lett.* **95**, 010402 (2005).
 - [26] S. Levy, E. Lahoud, I. Shomroni, and J. Steinhauer, *Nature* **449**, 579 (2007).
 - [27] D. T. Son and M. A. Stephanov, *Phys. Rev. A* **65**, 063621 (2002).
 - [28] V. M. Kaurov and A. B. Kuklov, *Phys. Rev. A* **71**, 011601(R) (2005).
 - [29] V. M. Kaurov and A. B. Kuklov, *Phys. Rev. A* **73**, 013627 (2006).
 - [30] A. Barone and G. Paterno, *Physics and Applications of the Josephson Effect* (Wiley and Sons Inc., 1982).
 - [31] S.-W. Su, S.-C. Gou, A. Bradley, O. Fialko, and J. Brand, *Phys. Rev. Lett.* **110**, 215302 (2013).
 - [32] V. Achilleos, J. Stockhofe, P. G. Kevrekidis, D. J. Frantzeskakis, and P. Schmelcher, *Europhys. Lett.* **103**, 20002 (2013).
 - [33] S. Cao, C.-J. Shan, D.-W. Zhang, X. Qin, and J. Xu, *J. Opt. Soc. Am. B* **32**, 201 (2015).
 - [34] J. Brand and W. P. Reinhardt, *J. Phys. B: At. Mol. Opt. Phys.* **34**, 4 (2001).
 - [35] A. Muñoz Mateo and J. Brand, *Phys. Rev. Lett.* **113**, 255302 (2014).
 - [36] M. Abad and A. Recati, *Eur. Phys. J. D* **67**, 148 (2013).
 - [37] T.-L. Ho and S. Zhang, *Phys. Rev. Lett.* **107**, 150403 (2011).
 - [38] M. I. Qadir, H. Susanto, and P. C. Matthews, *J. Phys. B: At. Mol. Opt. Phys.* **45**, 035004 (2012).
 - [39] A. Gallemí, A. Muñoz Mateo, R. Mayol, and M. Guilleumas, arXiv:1509.04418 (2015).
 - [40] S.-W. Su, S.-C. Gou, I.-K. Liu, A. S. Bradley, O. Fialko, and J. Brand, *Phys. Rev. A* **91**, 023631 (2015).
 - [41] D. Roditchev, C. Brun, L. Serrier-Garcia, J. C. Cuevas, V. H. L. Bessa, M. V. Milosevic, F. Debontridder, V. Stolyarov, and T. Cren, *Nat. Phys.* **11**, 332 (2015).
 - [42] E. A. Kuznetsov and S. K. Turitsyn, *Sov. Phys. JEPT* **67**, 1583 (1988).
 - [43] E. A. Kuznetsov and J. J. Rasmussen, *Phys. Rev. E* **51**, 4479 (1995).

- [44] G. Huang, V. A. Makarov, and M. G. Velarde, Phys. Rev. A **67**, 023604 (2003).
- [45] M. J. Ku, W. Ji, B. Mukherjee, E. Guardado-Sanchez, L. W. Cheuk, T. Yefsah, and M. W. Zwierlein, Phys. Rev. Lett. **113**, 065301 (2014).
- [46] M. J. Ku, B. Mukherjee, T. Yefsah, and M. W. Zwierlein, arXiv:1507.01047 (2015).
- [47] D. V. Freilich, D. M. Bianchi, A. M. Kaufman, T. K. Langin, and D. S. Hall, Science **329**, 1182 (2010).
- [48] R. Navarro, R. Carretero-González, P. J. Torres, P. G. Kevrekidis, D. J. Frantzeskakis, M. W. Ray, E. Altuntas, and D. S. Hall, Phys. Rev. Lett. **110**, 225301 (2013).